DOI: 10.5327/Z2317-48892013000300002

ARTICLE

Polycyclic evolution of Camboriú Complex migmatites, Santa Catarina, Southern Brazil: integrated Hf isotopic and U-Pb age zircon evidence of episodic reworking of a Mesoarchean juvenile crust

Evolução policíclica dos migmatitos do Complexo Camboriú, Santa Catarina, Sul do Brasil: retrabalhamento episódico da crosta juvenil Mesoarqueana revelada pelo estudo integrado de isótopos de Hf e idades U-Pb em zircão

Miguel Angelo Stipp Basei[1]*, Mario da Costa Campos Neto[1], Angela Pacheco Lopes[1], Allen Phillip Nutman[2], Dunyi Liu[3], Kei Sato[1]

ABSTRACT: Camboriú Complex is the only gneissic-migmatitic inlier within the Neoproterozoic Brusque Group supracrustal rocks, in the northernmost part of the Dom Feliciano Belt, Southern Brazil. It comprises Morro do Boi migmatites and diatexitic Ponta do Cabeço Granite. Zircon U-Pb dating of migmatites and associated granitic neosomes shows that the crustal evolution started in the Paleo-Mesoarchean (from 3.3 to 3.0 Ga), continued with events through the Neoarchean and Paleoproterozoic, and ended in the Neoproterozoic (from 0.64 to 0.61 Ga). Integration of zircon Hf isotopic data and U-Pb ages indicates that juvenile crustal accretion was restricted to the Archean and that, afterwards, the intracrustal reworking predominated. The exception to this is the *ca.* 1.56 Ga xenoliths (basic dike remnants?), whose magmatic zircons have juvenile Hf isotopic signatures. This basic magmatism marks an extension of the earlier Precambrian complex. Although the Camboriú Complex is dominated by early Precambrian crustal additions, it was so strongly reworked in the Neoproterozoic that melts derived from it intruded the adjacent Neoproterozoic Brusque Group supracrustal rocks. Due to this strong overprint, the Camboriú Complex is regarded as a Neoproterozoic (Ediacaran) geotectonic unit. In terms of its history, the Camboriú Complex most closely matches the Atuba Complex, the basement of Curitiba microplate that occurs further to the North, close to the Ribeira Belt, which is another Neoproterozoic orogen in Southern Brazil.

KEYWORDS: crustal evolution; Dom Feliciano Belt; migmatites; Hf isotopes; SHRIMP zircon ages.

RESUMO: *O Complexo Camboriú é a única ocorrência de rochas gnáissico-migmatíticas em meio às rochas supracrustais neoproterozoicas do Grupo Brusque, extremidade norte do Cinturão Dom Feliciano, Sul do Brasil. Compreende os migmatitos Morro do Boi e o diatexito Ponta do Cabeço. Dados U-Pb em zircão dos migmatitos bandados e dos neossomas graníticos associados mostram que a evolução crustal começou no Paleo-Mesoarqueano (de 3,3 a 3,0 Ga), continuou por meio de eventos no Neoarqueano e Paleoproterozoico e terminou no Neoproterozoico (de 0,64 a 0,61 Ga). Integração das idades U-Pb com os dados dos isótopos de Hf indica que a acreção juvenil foi restrita ao Arqueano e que, posteriormente, o retrabalhamento intracrustal predominou. A exceção é representada pelos xenólitos de anfibolitos em meio ao diatexito Ponta do Cabeço, cujos zircões magmáticos apresentaram assinaturas isotópicas juvenis. Este magmatismo básico marca uma extensão do Complexo Camboriú ao redor de 1,56 Ga. Apesar do Complexo Camboriú ser dominado por acreções juvenis arqueanas e frequentemente exibir zircão com núcleos herdados antigos, a intensidade do retrabalhamento sofrido por esse Complexo foi de tal magnitude que mobilizados associados a ele intrudem as rochas supracrustais neoproterozoicas do Grupo Brusque. Devido ao intenso retrabalhamento, o Complexo Camboriú é considerado uma unidade geotectônica neoproterozoica (Ediacarana). Em termos de sua história, este Complexo se assemelha ao Complexo Atuba, o qual representa o embasamento da Microplaca Curitiba que ocorre mais ao Norte, próximo ao Cinturão Ribeira, que é outro orógeno neoproterozoico no Sul do Brasil.*

PALAVRAS-CHAVE: *evolução crustal; cinturão Dom Feliciano; migmatitos; isótopos de Hf; idades U-Pb em zircão.*

[1]Geosciences Institute, University of São Paulo - USP, São Paulo (SP), Brazil. *E-mails: baseimas@usp.br; camposnt@usp.br; angelalopes@usp.br; keysato@usp.br*

[2]Research School of Earth Sciences - ANU, Canberra, Australia; School of Earth and Environmental Sciences, University of Wollongong, Wollongong, Australia. *E-mail: allen.nutman@gmail.com*

[3]Beijing SHRIMP Center, Chinese Academy of Geological Sciences, Beijing, China. *E-mail: liudunyi@bjshrimp.cn*

*Corresponding author

Manuscrito ID: 30019. **Recebido em:** 09/08/2013. **Aprovado em:** 09/08/2013.

INTRODUCTION

The Río de la Plata, Kalahari, and Congo cratons play a central role in the assembly of Western Gondwana, along the Neoproterozoic orogenic belts on both sides of the modern Southern Atlantic Ocean. These belts contain inliers of older gneissic rocks, which might be parautochthonous to the cratons of Western Gondwana in South America, or they might be exotic fragments of others, rafted in from further east in Gondwana by the closure of Neoproterozoic ocean basins. The Camboriú Complex is one of these fragments of uncertain provenance and long polycyclic history.

In this paper, we investigated the geological history of the Camboriú Complex via integrated field observations, zircon U-Pb dating, and Hf isotopic signatures. This revealed that in the Neoproterozoic there was reworking of early Precambrian components, without the addition of juvenile crustal material. Evidence of Paleoproterozoic reworking was also observed. The only post-Archean juvenile crustal additions seem to be the emplacement of basic dikes at 1.56 Ga, which are now found as dismembered amphibolite bodies due to the strong Neoproterozoic migmatization. The established detailed evolution of the Camboriú Complex is here compared and contrasted with that of other basement inliers in the Southern Brazilian Neoproterozoic orogenic belts.

GEOLOGICAL SETTING

The different crustal blocks in Southeastern South America were juxtaposed during the Neoproterozoic assembly of Western Gondwana (Fig. 1A). The Precambrian terranes of Santa Catarina belong to the Mantiqueira Structural Province (Almeida *et al*. 1981). They comprise two major geotectonic units: the Luis Alves microplate and its cover in the North, and the Dom Feliciano belt in the South. The former was stabilized in the Paleoproterozoic. The Neoproterozoic Dom Feliciano Belt extends from Southeastern Brazil into Uruguay, and has three major NNE-trending segments that were juxtaposed during the Neoproterozoic (Fig. 1B).

In Santa Catarina, the Dom Feliciano belt central segment includes the Brusque Group supracrustal rocks (Basei *et al*. 2000, Phillip *et al*. 2004), which separate the Florianópolis batholith granites to the South from Itajaí Group foreland basin. The latter occurs at the border of Luis Alves microplate gneissic-migmatitic terranes (Fig. 1).

The Camboriú Complex is located near the city of the same name in the Northeast of Santa Catarina (Fig. 1C). It is considered a basement inlier within the Brusque Group metavolcano-sedimentary sequence (Basei *et al*. 2000, 2005, 2008, 2010; Hartmann *et al*. 2003; Bittencourt & Nardi 2004, Phillip *et al*. 2009). It is well-exposed along road cuts and in coastal outcrops. Similar rocks can be found either within the Florianópolis Batholith granitoids or in the Itajaí Group supracrustal rocks, suggesting that it might be an exotic terrane. It is composed of banded gneisses and migmatites named Morro do Boi migmatites (Basei 1985, Basei *et al*. 2000). They have banded gneiss paleosomes of alternating centimeter-sized gray and white quartzo-feldspathic bands. The neosome comprises centimeter-sized leucocratic bands of predominantly granodioritic composition. The other Camboriú Complex constituent is Ponta do Cabeço Granite, which is a medium to light-gray diatexitic granitoid that contains a profusion of mafic xenoliths, making it distinctive in the field. Neosome of Morro do Boi migmatites might be gradational into Ponta do Cabeço Granite. Late, irregular, meter-sized leucocratic granitoid sheets crosscut the migmatitic banding, and form sheets that are sub-parallel to the migmatitic structures.

PONTA DO CABEÇO GRANITE

Ponta do Cabeço Granite is, in fact, a schollen-structured diatexite and is the most voluminous component of the Camboriú Complex. It has a hook shape in the northeast end of Valsungana batholith (Fig. 1C). Its composition is of monzogranitic to syenogranitic, bearing biotite ± subordinate hornblende. This granite is gray, with fine- to coarse-equigranular texture, and grain-size banding parallel to the relic compositional banding (Figs. 3A and B). It shows a regional preferential NE-SW fabric defined by the alignment of mafic enclaves. The granite grades into Ponta do Cabeço diatexite, which in turn performs it into Morro do Boi migmatites. Its predominant structures are schollen and schlieren, which may take place in the same outcrop (Fig. 3B). Both igneous and metamorphic micro-textures are observed with variations from inequigranular to granoblastic and locally lepidogranoblastic.

The abundance of enclaves is a distinctive characteristic of Ponta do Cabeço granite. They have varied compositions and are up to 1 m across (orthogneiss, amphibolite, pyroxenite, biotitite, and calc-silicate rocks), with fine to medium-grain size. The predominant enclave type is amphibolite. Relicts of metamorphic clinopyroxene in the hornblende are locally preserved.

Two metamorphic events may be suggested, one of upper amphibolite facies with the formation of clinopyroxene,

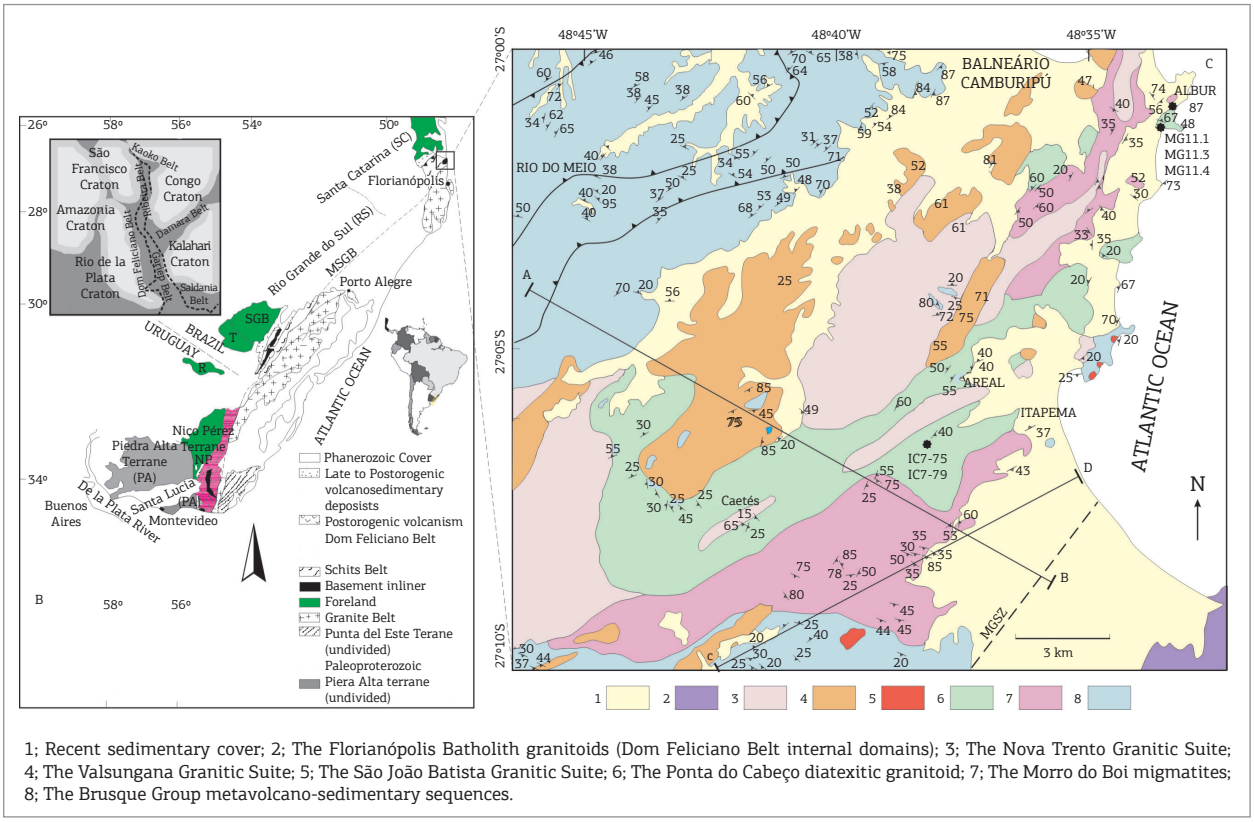

Figure 1. (A) Sketch map showing the position of the major Neoproterozoic cratons and fold belts during the formation of Western Gondwana. (B) Sketch of the geological map of Dom Feliciano Belt (simplified from Basei *et al.* 2011). (C) Geological map of the Camboriú Complex.

and a medium one including the development of hornblende with partial breakdown of clinopyroxene. The enclaves have sharp to gradational margins with reaction rims. Some banded migmatite enclaves present folded banding, indicating they were deformed before the emplacement of Ponta do Cabeço Granite.

The voluminous Ponta do Cabeço diatexite of mainly granitic composition lies at the base of the Camboriú Complex. This forms a southwest dipping anti-form with *ca.* 8 km wavelength (Fig. 2, section AB). It is intruded by the homogeneous porphyritic biotite-bearing Valsungana granite, and thick NE-oriented bodies of Nova Trento Suite, which are leucocratic, medium-grained, isotropic granite.

Feldspar megacrysts in the diatexite are euhedral and oriented, resulting in a sub-magmatic foliation and in a parallel compositional banding (Fig. 3A). The foliation deflects around competent mafic rafts with local development of strain shadow zones, in which there is coarse-grained white granite or fine-grained gray granite/granodiorite. These structures suggest that the migmatite experienced a syn-magmatic flow related to regional deformation. Biotite or hornblende and biotite schlieren can grade into amphibolite schollen. The neosome assemblage is plagioclase plus quartz plus K-feldspar plus biotite ± hornblende with accessory allanite armored by the epidote.

The paleosome schollen (*sensu* Sawyer, 2008a, b) has a rectangular to roundish form and is centimeter to submetric-sized, mostly oriented or stretched into the flow foliation. The schollens are predominantly melanocratic rocks such as amphibolite, biotite metatexite, biotite-hornblende metatexite, and resisters of ultramafic rocks and calc-silicate gneisses. These are heterogeneously affected by partial melt segregation during the flow of the diatexite magma (Fig. 4A), producing an internal incipient net-structured leucosome, or being consumed by diatexitic melt in strain-shadow zones.

MORRO DO BOI MIGMATITES

Morro do Boi migmatites are metatexitic rocks, in which stromatic structures predominate. The unit is cut by the Nova Trento, Valsungana, and Morro do Boi granites and crops out in the limbs of a late NE-oriented anti-form, which includes Ponta do Cabeço Diatexite in its core (Fig. 2, sections AB and CD).

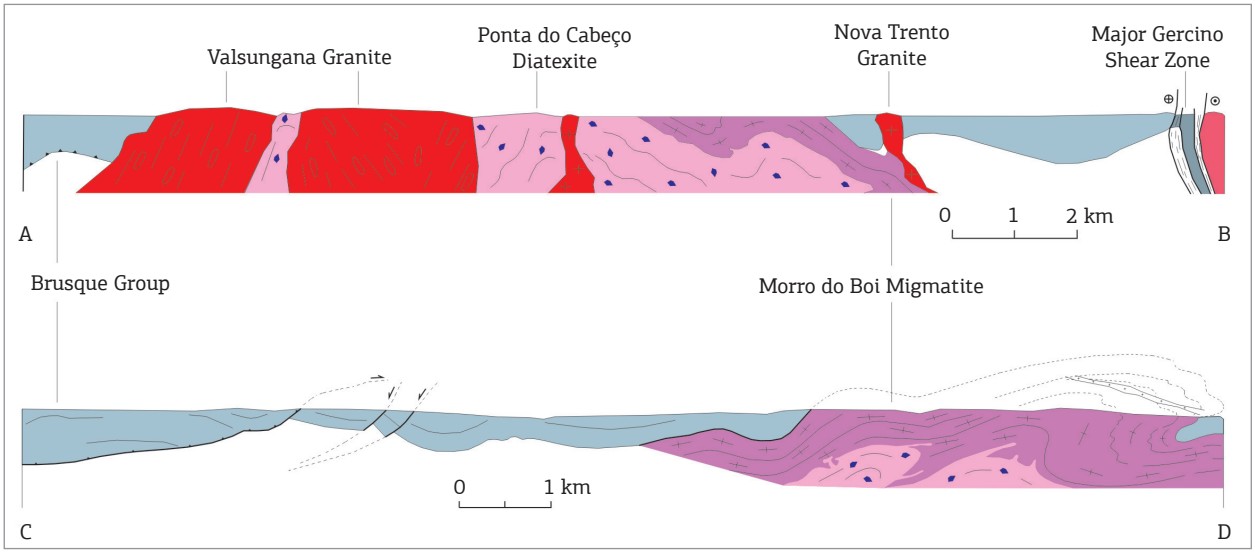

Figure 2. Geological cross-sections AB and CD (position indicated in Fig. 1).

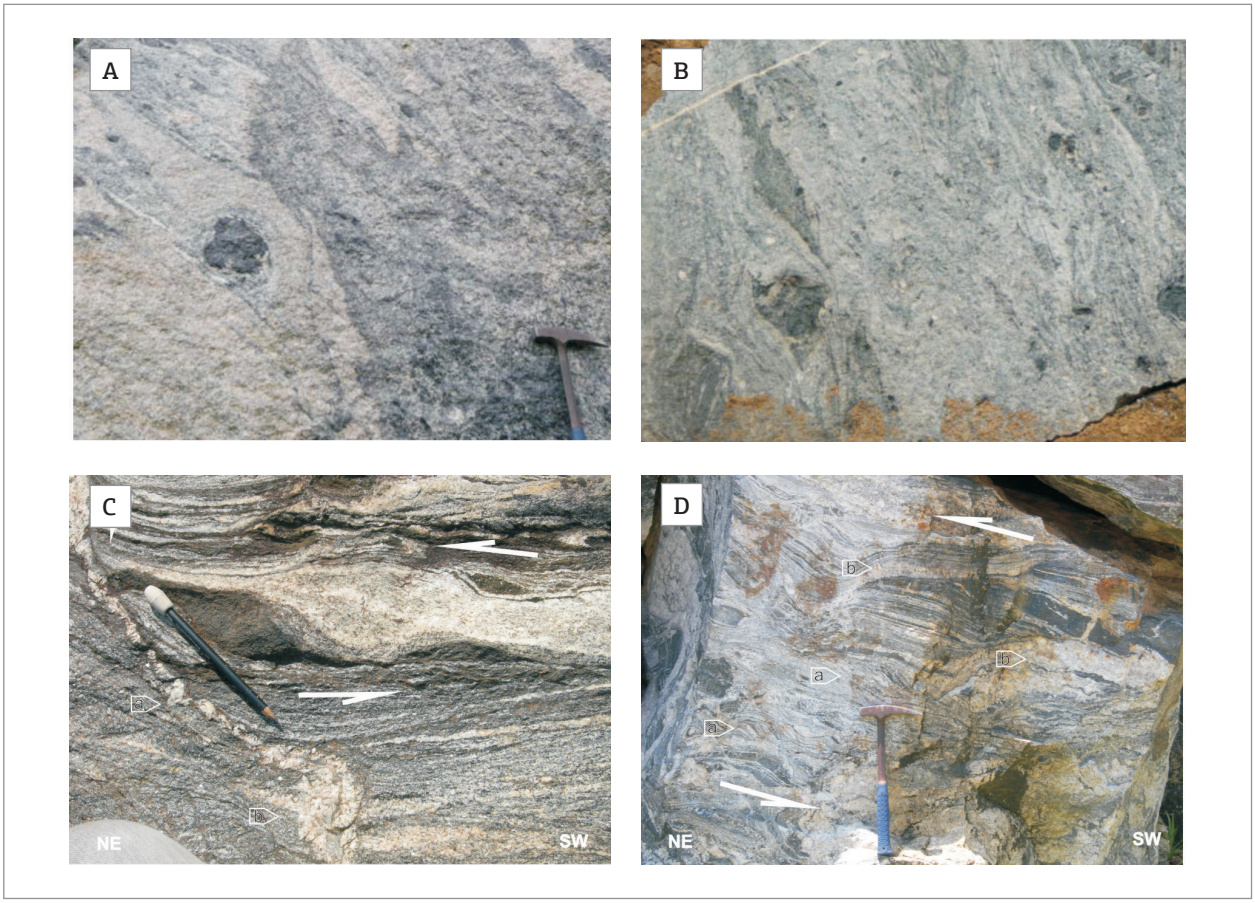

Figure 3. (A) Ponta do Cabeço amphibolite schollen-bearing diatexite with compositional banding and ghost nebulitic layers. (B) Ponta do Cabeço diatexite with folded compositional banding and schollen with triangular pressure shadow zones filled with diatexite. (C) Hornblende-biotite metatexite with centimeter-sized boudins of amphibolite. The asymmetrical stair-stepping shape of leucosome and resisters of gray amphibolite boudins indicate low-angle transport towards NE along the transposition foliation. A pink feldspathic vein filling an extensional shear has an opposite sense of movement. It was stretched and folded with the main transposition foliation in the axial plane position: boudins of feldspathic veins and a folded vein with injection into the main transposition foliation. (D) Pale hornblende + biotite bearing diatexite, with schollen, schilieren, compositional banding, and folded pink veins of granitic composition filling shear bands. Note the syn-anatectic S-C foliation (A) and C' shear-bands (B). The sense of flow is indicated.

Most of its migmatites have folded layering on a 1 – 4-cm scale, which locally grades into agmatitic and more rarely nebulitic domains (Fig. 3C). The migmatite paleosome is mostly tonalitic to granodioritic, within which centimeter- to decimeter-thick amphibolitic bodies are found. Some of these retain tabular shapes reminiscent of dismembered dikes (Figs. 4A and D), whilst others are boudinaged and rounded. These are frequently enveloped and cut by granitic neosome. Locally, biotite selvedges separate the neo- and paleosomes (Fig. 4C), suggesting they were generated by *in situ* melting. Invaginated within the dominant tonalitic-granodioritic paleosomes, there are some sillimanite-bearing metapelitic units.

The gneiss foliation and stromatic leucosomes were intensively folded in a set of decimeter- and meter-sized parasitic folds (axial hinge lines varying from S to S65 W) on a major asymmetrical, SE-verging cylindrical anti-form. This fold preserves its upper limb and hinge zone, however the lower limb has been transposed/removed into an axial-planar ductile thrust (Fig. 2, section CD).

The syn-anatectic foliation coincides with a S60W-trending-fold axial mineral lineation, sheath-folds and S-C fabric sigmoidal leucosomes. It shows that flow of the anatectic rocks was at a shallow angle towards the NE (Fig. 2), essentially along the trend of the orogenic belt. All of these Neoproterozoic migmatite structures predate intrusion of

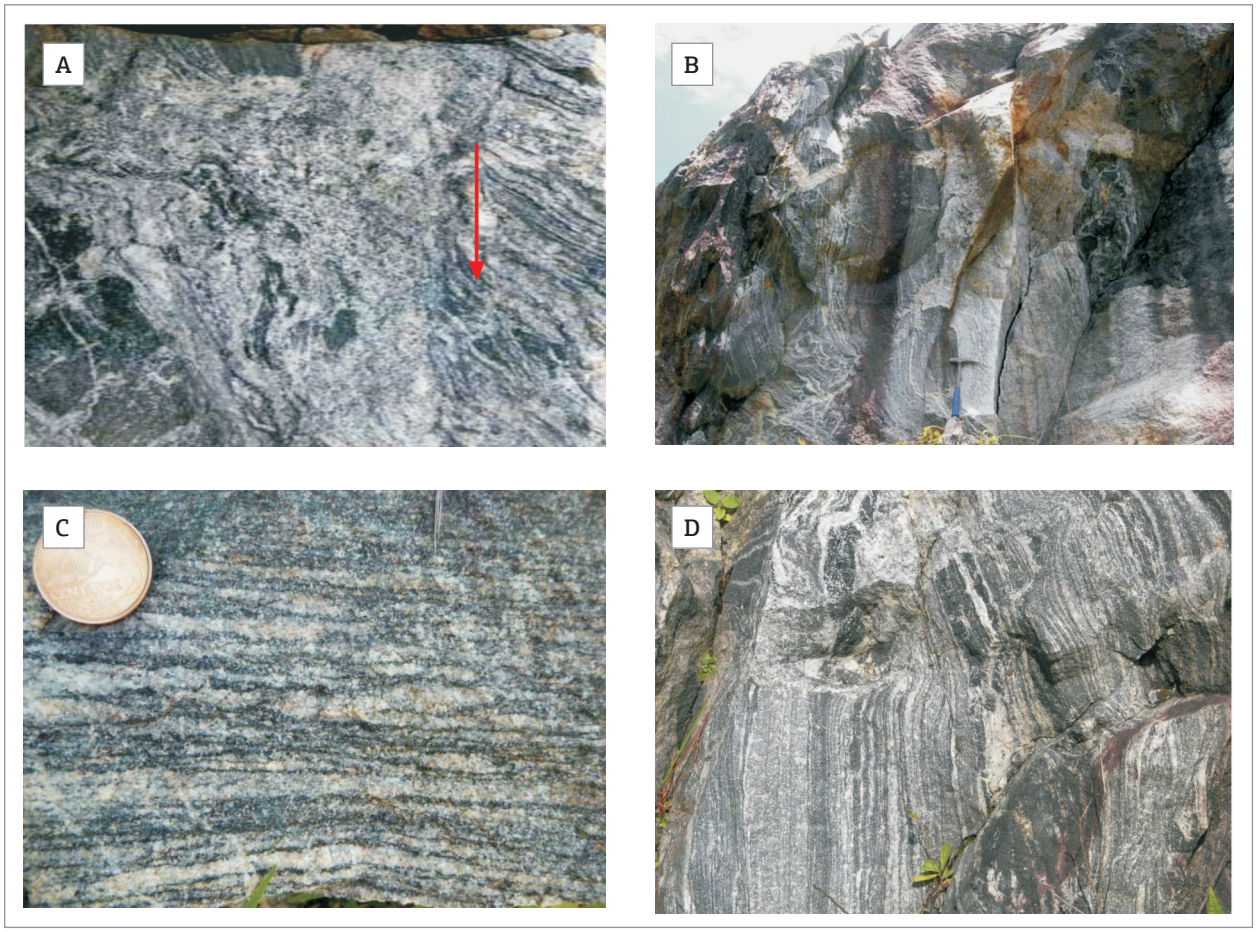

Figure 4. (A) Schollen-structured biotite-hornblende diatexite-metatexite transition with many elongated schollen of amphibolite as boudin, resisters, or paleosome. Two main domains of diatexite could be observed: left side – medium-grained trondhjemitic leucosome, which is interlayered with thin discontinuous layers of hornblende-rich paleosome as schlieren and boudins of more resistant amphibolite schollens; central – pale coarse-grained inequigranular diatexite within dilation structures. This diatexite was developed, in contrast to the other type, in the interior of a normal shear zone; right side – coarse-grained and irregular stromatic layers with melanosome selvedges occurring parallel to the schilieren and compositional banding. (B) Tonalite dike exhibiting ghost compositional banding that resembles a nebulitic diatexite. It is intrusive in the main migmatitic structures of the metatexite. (C) Typical stromatic banding in biotite tonalite-granodiorite gneisses. Note that around the quartzo-feldspathic bands, there are selvedges of mafic minerals. (D) Banded hornblende-biotite tonalitic gneiss with variable among of titanite and allanite armored by epidote. Mesocratic amphibolite occurs as layers or boudins up to 10 cm thick.

the Valsungana Batholith and Nova Trento isotropic granite bodies (Basei *et al*. 2000, Silva *et al*. 2003, Vlach *et al*. 2009).

In the migmatites, epidote is always present in the clinopyroxene-free melt phase, suggesting a maximum temperature of around 700ºC and a minimum pressure of about 8 kbar (Poli & Schmidt 2004, Patiño Douce 2005).

PREVIOUS GEOCHRONOLOGICAL RESULTS

Paleoproterozoic to Neoproterozoic ages from the Camboriú Complex have been a matter of controversy. Basei (1985) reported a poorly-fitted Rb-Sr isochron with an Archean age of *ca*. 2.6 Ga for the Morro do Boi migmatites. Based on structural relations and on *ca*. 0.60 Ga K-Ar biotite, the author suggested a ductile reworking of ancient basement rocks in the Neoproterozoic *Brasiliano* orogeny.

Based on SHRIMP U-Pb zircon analyses, Silva *et al*. (2000), Hartmann *et al*. (2003) and Bitencourt & Nardi (2004) assigned the Camboriú Complex a Paleoproterozoic age based on *ca*. 2.2 Ga zircon cores. They regarded the Neoproterozoic ages for zircon overgrowths as an indication of superimposed hydrothermal, not igneous, processes. On the other hand, based on the zircon U-Pb 0.58 Ga lower concordia intercept age for the Ponta do Cabeço granitoid, Basei *et al*. (2000) questioned the interpretation of the previous authors and proposed that the main migmatization phase of the Camboriú Complex with generation of this granitoid occurred in the Neoproterozoic. Silva *et al*. (2005a, b) also reinterpreted them and noted the importance of Neoproterozoic events in the genesis of the Camboriú Complex granites.

ANALYTICAL PROCEDURES FOR ZIRCON SHRIMP U-PB AGES AND HF ISOTOPES

Zircons were separated using the conventional heavy liquid and isodynamic techniques. Selected zircons were mounted in epoxy resin together with the reference zircon Temora ($^{206}Pb/^{238}U$ age = 417 Ma), and then polished to expose the internal crystal texture. Prior to analysis, cathodoluminescence (CL) and transmitted and reflected light images were obtained in order that analysis sites could be chosen (McClaren *et al*. 1994). Following the CL images, the samples were cleaned and vacuum-coated with high-purity gold. Age determinations by SHRIMP were performed at the Research School of Earth Sciences (ANU, Canberra, Australia) and in the Beijing SHRIMP Center (CAGS, Beijing, China), according to standard procedures (Compston *et al*. 1984, Williams 1998, Stern 1998, Sircombe 2000). With the aim of increasing confidence in the accuracy of the U-Pb calibration, Temora grains were distributed as several clusters in different parts of the epoxy mount.

Zircons from the felsic rocks are prismatic, colorless, and transparent. The lengths of these crystals range from 250 to 80 μm, with aspect ratios of 5:1 to 2:1. In CL images, most of them display some oscillatory or linear zoning which is typical of magmatic zircon (Figs. 5 and 6). In many samples, there is a complex recrystallisation and/or development of overgrowths. These were methodically explored in the U-Pb geochronology in order to establish the complete high temperature tectonothermal history. Grains are weakly zoned with low luminescence. Zircons from the amphibolite xenoliths exhibit low luminescence, are unzoned to weakly zoned, and show a distinct internal spongy structure (Fig. 6).

All zircon data are shown in Tabela 1. Most of these yielded close to concordant ages. Pieces of information are represented in Concordia and Tera Wasserburg plots generated by the program Isoplot/Ex (Ludwig 2001). They were filtered before calculating ages to remove analyses with the most disturbed radiogenic Pb-systematics and with >2.5% ^{206}Pb of common origin, calculated from measured ^{204}Pb using Cumming and Richards' (1975) model Pb compositions.

Lu-Hf analyses were carried out at the Institute of Geosciences, University of São Paulo, on a Neptune laser-ablation multi-collector inductively coupled plasma mass spectrometer equipped with a Photon laser system (Sato *et al*. 2010). Apart from two analyses, the remaining 79 Lu-Hf isotopic analyses reported here were performed on the same zircon domains that were previously U-Pb dated by SHRIMP. The laser spot used was 39 μm in diameter with an ablation time of 60 seconds, repetition rate of 7 Hz, and He used as the carrier gas (Sato *et al*. 2009, 2010).

$^{176}Hf/^{177}Hf$ ratios were normalized to $^{179}Hf/^{177}Hf = 0.7325$. Zircon Hf isotopic data are presented in Tabela 2. The isotopes ^{172}Yb, ^{173}Yb, ^{175}Lu, ^{177}Hf, ^{178}Hf, ^{179}Hf, ^{180}Hf, and $^{176}(Hf+Yb+Lu)$ were simultaneously collected. $^{176}Lu/^{175}Lu$ ratio of 0.02669 was used to calculate $^{176}Lu/^{177}Hf$. Mass bias corrections of Lu-Hf isotopic ratios were done applying the variations of GJ1 standard. A decay constant for ^{176}Lu of 1.867×10^{-11} a^{-1} (Söderlund *et al*. 2004), the present-day chondritic ratios of $^{176}Hf/^{177}Hf = 0.282772$ and $^{176}Lu/^{177}Hf = 0.0332$ (Blichert-Toft & Albarede 1997) were adopted to measure ε_{Hf} values. A two-stage continental model (T_{DM2}) was calculated using the initial $^{176}Hf/^{177}Hf$ of zircon and the $^{176}Lu/^{177}Hf = 0.022$ ratio for the lower continental crust (Griffin *et al*. 2004).

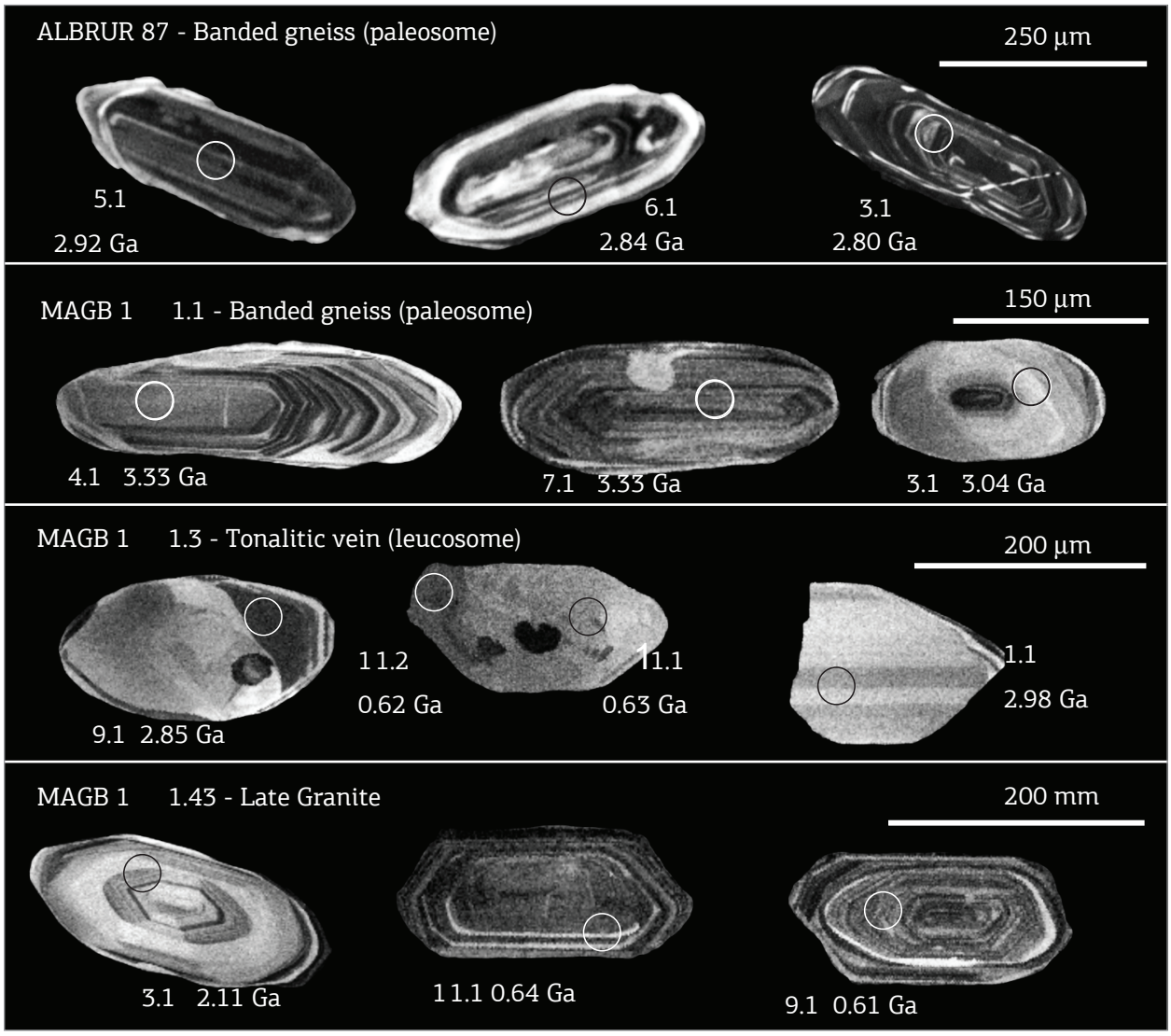

Figure 5. Cathodoluminescence images of selected zircons from the Morro do Boi migmatites and late granite.

U-PB RESULTS

Paleosome of Morro do Boi migmatites

Zircons from MAGB 11.1 sample (representative CL images in Fig. 5, summary concordia diagram in Fig. 7A) yielded Archean $^{207}Pb/^{206}Pb$ ages, which cluster at *ca*. 3.3 Ga (cores) and 3.0 Ga (overgrowths). Both groups have a dispersion in $^{207}Pb/^{207}Pb$ beyond analytical error, and yield weighted mean $^{207}Pb/^{206}Pb$ ages of 3,319 ± 29 Ma (MSWD = 2.3) and 3,022 ± 32 Ma (MSWD = 3.2) respectively. Paleoproterozoic zircon growth was also present with concordant ages yielding a weighted mean $^{207}Pb/^{206}Pb$ age of 2,050 ± 56 Ma (MSWD = 0.7). Zircons with neoproterozoic ages were not detected in the paleosome samples.

The sample ALBRUR 87 resulted in a single population defined by prismatic zircons with rounded terminations (representative CL images in Fig. 5, summary concordia diagram in Fig. 7B). All analyses had discordant ages, but they seem to form a single *ca*. 2.9 Ga population that suffered variable degrees of ancient loss of radiogenic Pb. They present a poorly defined $^{207}Pb/^{206}Pb$ weighted average age of 2,901 ± 41 Ma (MSWD = 38). Neither *ca*. 3.3 Ga cores nor Neoproterozoic zircons were detected.

Neosome of Morro do Boi migmatites

Sample MAGB 11.3 represents a typical pale neosome vein of tonalitic composition that occurs within the banded migmatites. It is ca. 15 cm thick and it was foliated and folded together with the paleosome. CL images of representative zircons are shown in Fig. 5 and results are summarized in a concordia diagram in Fig. 8. Structural cores of zircons yielded concordant Mesoarchean ages with a weighted mean

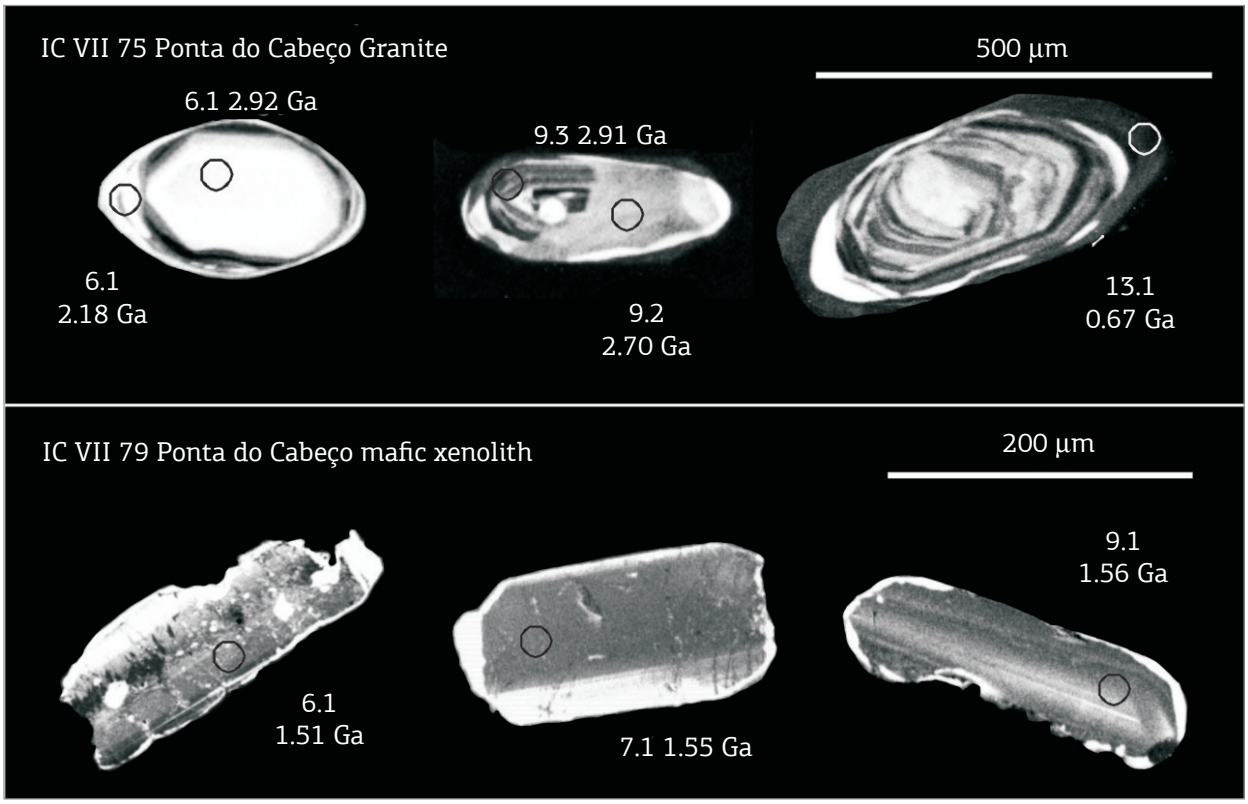

Figure 6. Cathodoluminescence images of selected zircons from Ponta do Cabeço diatexite and from a mafic xenolith.

$^{207}Pb/^{206}Pb$ age of 2,980 ± 20 Ma (MSWD = 0.7), similar in age to some paleosome zircon components. Four determinations on rims provided concordant ages with a weighted mean $^{206}Pb/^{238}U$ age of 634 ± 24 Ma (MSWD = 0.2). The results suggest that the leucosome is originated from the Neoproterozoic melting of Archean paleosomes. This conclusion has also been said by Lopes (2008), based on whole-rock Sr and Nd isotopic data.

Ponta do Cabeço Granite

A total of 18 analyses was undertaken on zircons from sample IC VII 75 of the Ponta do Cabeço diatexite matrix (CL images of representative zircons in Fig. 6; results are summarized in a concordia diagram in Fig. 9A). The structural cores are not all of the same age. The earliest generation is Mesoarchean, which is close to concordant ages at 3.0 – 2.9 Ga. A second generation of structural cores, apparently replacing 3.0 – 2.9 Ga zircon (Fig. 6), is formed at *ca*. 2.7 Ga. Another episode of zircon growth/recrystallization occurred at 2.0 – 1.9 Ga. In all cases, these domains are disturbed with $^{207}Pb/^{206}Pb$ ages dispersing well beyond the analytical error. Despite this, one may still conclude that three generations of early Precambrian zircon growth are present (Fig. 9A). Overgrowths forming the outmost rims yield concordant ages, with a weighted mean $^{206}Pb/^{238}U$ age of 637 ± 21 Ma (MSWD = 0.30). These are interpreted as the age of Neoproterozoic anatexis.

Amphibolite xenolith in Ponta do Cabeço Granite

Zircons from an amphibolite enclave sample IC VII 79 are rich in micro-inclusions (Fig. 6) and show high Th/U ratios of > 0.6. These are both common features of gabbro magmatic zircons. Except for one analysis, they form a single population showing variable degrees of discordance, with $^{207}Pb/^{206}Pb$ ages dispersed beyond the analytical error (Fig. 9B). Also, they result in a weighted mean $^{207}Pb/^{206}U$ age of 1,563 ± 25 Ma (MSWD = 7.8), which is interpreted as the best age estimate of igneous emplacement of a gabbroic protolith. One anomalous zircon analysis yielded a Neoproterozoic age and a distinctly lower Th/U of 0.2. This means a recrystallisation domain formed during superimposed Neoproterozoic tectonothermal activity.

Granite dike cross-cutting migmatite structures

A dike of leucocratic granite crosscutting the banded migmatites (MAGB 11.4) showed complex zircons (CL

Table 1. SHRIMP U-Pb zircon analytical data for Camboriú Complex rocks. Analytical errors are given at the one-sigma level

Labels	Site	U/ppm	Th/ppm	Th/U	Pb*/ppm	204/ppb	f206	Ratios and errors						Ages and Errors				Conc
								206 Pb/238 U	Error	207 Pb/235 U	Error	207 Pb/206 Pb	Error	206 Pb/238 U	Error	207 Pb/206 Pb	Error	%
ALBRUR 87 - Morro do Boi Migmatite (banded gneiss - mesosome)																		
1.1	e,osc,d,p	1541.2	809.1	0.52	429	290	0.0118	0.24238	0.00616	7.24508	0.19707	0.21680	0.00152	1399	32	2957	11	47
2.1	e,osc,p	419.4	94.5	0.23	194	3	0.0002	0.43501	0.01368	10.43332	0.33957	0.17395	0.00093	2328	62	2596	9	90
3.1	c,osc,p	549.1	117.1	0.21	281	3	0.0002	0.47582	0.01344	13.68911	0.41344	0.20866	0.00162	2509	59	2895	13	87
4.1	c,osc,p,fr	513.4	528.4	1.03	316	21	0.0014	0.46704	0.01847	13.61508	0.55271	0.21143	0.00115	2471	82	2917	9	85
5.1	c,osc,hd,p	1329.1	217.2	0.16	700	101	0.0024	0.49030	0.01337	14.33691	0.39860	0.21208	0.00063	2572	58	2921	5	88
6.1	e,osc,p	501.4	389.2	0.78	252	24	0.0017	0.43045	0.01155	11.98405	0.33042	0.20192	0.00078	2308	52	2842	6	81
7.1	c,osc,p	523.8	235.0	0.45	235	4	0.0003	0.38185	0.01769	11.40078	0.53708	0.21654	0.00097	2085	83	2955	7	71
8.1	e,osc,p	796.7	77.4	0.10	424	4	0.0002	0.50430	0.01363	14.20047	0.39493	0.20423	0.00081	2632	59	2860	7	92
MAGB 11.1 - Morro do Boi Migmatite (banded gneiss - mesosome)																		
1.1	e,h/rex,p	29.6	34.3	1.16	13	24	0.0332	0.34584	0.01261	5.75482	0.40292	0.12069	0.00668	1915	61	1966	102	97
2.1	e,h/rex,p	102.6	91.3	0.89	42	14	0.0059	0.33909	0.01530	5.51292	0.37322	0.11791	0.00532	1882	74	1925	83	98
3.1	e,h/rex,p	38.6	36.6	0.95	30	12	0.0073	0.61166	0.02023	19.20089	0.77449	0.22767	0.00440	3077	81	3036	31	101
4.1	m,osc,p	250.4	133.3	0.53	206	15	0.0013	0.67478	0.02808	25.51517	1.09759	0.27424	0.00189	3324	109	3330	11	100
5.1	m,osc,p	109.1	53.9	0.49	93	27	0.0049	0.70587	0.02249	26.05785	0.89886	0.26774	0.00263	3443	86	3293	15	105
6.1	m,osc,p	147.1	84.9	0.58	107	19	0.0031	0.59966	0.02818	21.22629	1.04792	0.25672	0.00266	3028	115	3227	16	94
7.1	e,osc,p	172.9	83.5	0.48	148	21	0.0025	0.70885	0.02517	26.74032	0.98249	0.27359	0.00164	3454	96	3327	9	104
8.1	m,osc,p	199.1	196.5	0.99	141	27	0.0035	0.55265	0.03188	16.98039	0.99651	0.22284	0.00128	2836	134	3001	9	95
9.1	e,h,p,r	104.1	35.2	0.34	64	13	0.0034	0.52988	0.02678	16.19778	0.89712	0.22171	0.00381	2741	114	2993	28	92
10.1	e,h,l,p	68.0	21.5	0.32	40	20	0.0080	0.52610	0.02058	15.38746	0.65248	0.21213	0.00258	2725	88	2922	20	93
11.1	e,h,l,p	117.5	103.6	0.88	73	31	0.0082	0.46210	0.02287	13.76992	0.72062	0.21612	0.00258	2449	102	2952	19	83
12.1	e,h,d,p	105.3	75.5	0.72	44	15	0.0056	0.36582	0.01359	6.40475	0.27226	0.12698	0.00210	2010	64	2057	30	98
13.1	e,h,d,p	81.1	97.9	1.21	61	11	0.0036	0.56230	0.01863	17.66955	0.64725	0.22791	0.00274	2876	77	3037	19	95
14.1	c,osc,r	179.9	132.2	0.73	119	31	0.0045	0.53678	0.03823	16.99536	1.23116	0.22963	0.00162	2770	162	3050	11	91
15.1	c,osc,r	156.3	89.7	0.57	129	12	0.0016	0.67911	0.02146	25.04335	0.88026	0.26746	0.00319	3341	83	3291	19	102
MAGB 11.3 - Morro do Boi Migmatite (tonalitic vein - leucosome)																		
1.1	c,osc,p	37.5	25.4	0.68	26	8	0.0078	0.58665	0.02387	17.75496	0.80247	0.21950	0.00334	2976	98	2977	25	100
2.1	e,h,p	85.7	0.2	0.00	7	4	0.0103	0.09507	0.00379	0.79968	0.06586	0.06100	0.00410	585	22	639	152	92
3.1	c,h,ov	62.3	48.3	0.78	41	10	0.0060	0.53265	0.01824	15.98508	0.59778	0.21766	0.00247	2753	77	2963	18	93
4.1	e,h,ov	2130.2	1056.7	0.50	123	370	0.0546	0.06235	0.00250	0.47419	0.03124	0.05516	0.00262	390	15	419	110	93
5.1	m,h,rp	44.2	72.0	1.63	35	12	0.0098	0.55815	0.02262	16.80908	0.77838	0.21842	0.00391	2859	94	2969	29	96
6.1	m,osc,p	52.2	41.4	0.79	12	5	0.0099	0.20366	0.01143	2.31569	0.17016	0.08246	0.00337	1195	62	1257	82	95
7.1	m,h,p	133.1	80.8	0.61	91	9	0.0024	0.57264	0.03008	17.52955	0.95654	0.22202	0.00213	2919	125	2995	15	97
6.2	e,osc,p	335.8	82.4	0.25	51	120	0.0463	0.15326	0.00739	1.40748	0.11151	0.06661	0.00380	919	41	825	124	111
8.1	r,hd,p	2827.9	176.2	0.06	101	175	0.0318	0.03912	0.00250	0.26634	0.02325	0.04938	0.00257	247	16	166	127	149
9.1	rex,h,p	432.7	11.8	0.03	216	16	0.0016	0.47916	0.02094	13.40916	0.61225	0.20296	0.00179	2524	92	2850	14	89
2.2	e,h,p	162.4	0.4	0.00	16	1	0.0014	0.10481	0.00318	0.87683	0.03579	0.06067	0.00144	643	19	628	52	102
10.1	e,h,p	126.1	30.8	0.24	33	13	0.0091	0.23603	0.02267	4.48053	0.48443	0.13767	0.00537	1366	119	2198	69	62
11.1	e,h,p	48.0	0.0	0.00	5	5	0.0208	0.10295	0.00399	0.88557	0.13525	0.06239	0.00892	632	23	687	339	92
11.2	e,h,p	97.0	0.7	0.01	9	10	0.0215	0.10192	0.00363	0.84298	0.08272	0.05999	0.00522	626	21	603	201	104
IC VII 75 - Ponta do Cabeço Leucogranite																		
1.1	e,r,br,p/r	65.9	13.1	0.20	37	1	0.0006	0.51776	0.03091	14.61917	0.98803	0.20478	0.00514	2690	133	2865	41	94
2.1	e,r,br,p/r	340.5	41.9	0.12	30	39	0.0186	0.09213	0.00481	0.82239	0.06625	0.06474	0.00357	568	28	766	121	74
3.1	e,r,br,p/r	266.3	33.3	0.13	40	88	0.0330	0.14618	0.00633	2.03806	0.12565	0.10112	0.00392	879	36	1645	74	54
4.1	e,osc,p	297.8	97.4	0.33	107	3	0.0004	0.33900	0.00839	6.01861	0.16849	0.12876	0.00133	1882	41	2081	18	90
5.1	e,r,br,p/r	207.8	26.0	0.13	36	34	0.0147	0.16866	0.00949	2.76590	0.17505	0.11894	0.00271	1005	53	1940	41	52
6.1	c,br,p/r	52.3	66.3	1.27	38	3	0.0015	0.54688	0.01659	15.92047	0.60989	0.21113	0.00420	2812	70	2914	33	97
6.2	e,br,r,p/r	79.6	9.0	0.11	28	2	0.0008	0.35327	0.01197	6.62201	0.27420	0.13595	0.00271	1950	57	2176	35	90

Continue...

Table 1. Continuation

Labels	Site	U/ppm	Th/ppm	Th/U	Pb*/ppm	204/ppb	f206	Ratios and errors						Ages and Errors				Conc
								206 Pb/238 U	Error	207 Pb/235 U	Error	207 Pb/206 Pb	Error	206 Pb/238 U	Error	207 Pb/206 Pb	Error	%
7.1	c,osc,d	183.0	115.7	0.63	128	1	0.0001	0.58500	0.01592	17.59956	0.51405	0.21819	0.00169	2969	65	2967	13	100
8.1	c,d,p/r	250.4	20.0	0.08	98	1	0.0002	0.39348	0.01009	7.35825	0.19705	0.13563	0.00070	2139	47	2172	9	99
9.1	e,h,p,rex	193.8	26.4	0.14	106	3	0.0004	0.51968	0.00985	13.32428	0.28356	0.18596	0.00141	2698	42	2707	13	100
9.2	e,h,p,rex	175.2	26.2	0.15	97	1	0.0001	0.52753	0.01230	13.45884	0.33403	0.18504	0.00113	2731	52	2699	10	101
9.3	c,osc,p	270.1	107.4	0.40	182	0	0.0000	0.59341	0.01172	17.19760	0.36713	0.21019	0.00126	3003	48	2907	10	103
10.1	m,h,br,rex,eq	31.8	48.2	1.51	16	1	0.0016	0.37326	0.01876	6.48922	0.37672	0.12609	0.00296	2045	89	2044	42	100
11.1	m,h,br,rex,eq	30.3	56.6	1.87	16	1	0.0010	0.35863	0.01370	6.11364	0.29090	0.12364	0.00297	1976	65	2009	43	98
12.1	h,d,p,r	1080.5	130.9	0.12	105	10	0.0013	0.10315	0.00205	0.83796	0.02025	0.05892	0.00068	633	12	564	25	112
7.2	h,d,p,r	522.3	71.3	0.14	52	24	0.0065	0.10497	0.00502	0.84765	0.05071	0.05857	0.00179	643	29	551	68	117
13.1	h,d,p,r	670.2	63.9	0.10	68	8	0.0017	0.10789	0.00614	0.89572	0.05591	0.06021	0.00118	660	36	611	43	108
7.3	r,h,br,rex,p	60.0	84.7	1.41	48	1	0.0005	0.57809	0.01452	17.20013	0.50073	0.21579	0.00257	2941	60	2950	19	100
IC VII 79 - Ponta do Cabeço Granite (mafic xenolith)																		
1.1	m,osc,fr	362.7	191.3	0.53	105	0	0.0000	0.26898	0.01230	3.53406	0.16841	0.09529	0.00085	1536	63	1534	17	100
2.1	m,osc,fr	89.5	36.5	0.41	25	4	0.0035	0.26941	0.01185	3.52585	0.17886	0.09492	0.00193	1538	60	1526	39	101
3.1	r,hb,fr	117.6	78.1	0.66	35	2	0.0013	0.27001	0.01254	3.63380	0.17737	0.09761	0.00101	1541	64	1579	19	98
4.1	m,hd,eq	2165.4	479.6	0.22	200	2	0.0002	0.09530	0.00415	0.78363	0.03484	0.05964	0.00030	587	24	590	11	99
6.1	e,osc/rex,p/anh	293.1	200.4	0.68	79	3	0.0008	0.24161	0.00706	3.13706	0.09764	0.09417	0.00072	1395	37	1512	15	92
7.1	m,h/osc,p	330.0	260.2	0.79	93	1	0.0003	0.24383	0.00871	3.22819	0.11863	0.09602	0.00051	1407	45	1548	10	91
8.1	e,osc,p,fr	260.3	129.8	0.50	73	1	0.0003	0.26345	0.00602	3.47477	0.08838	0.09566	0.00083	1507	31	1541	16	98
9.1	e,osc,p,fr	481.5	259.2	0.54	136	3	0.0005	0.26191	0.00900	3.49945	0.12570	0.09691	0.00068	1500	46	1565	13	96
10.1	m,osc,p,fr	150.8	74.1	0.49	39	4	0.0025	0.24554	0.00808	3.16395	0.11386	0.09346	0.00103	1415	42	1497	21	95
11.1	m,osc,p,fr	334.3	320.2	0.96	89	2	0.0006	0.22120	0.00736	2.82605	0.09793	0.09266	0.00059	1288	39	1481	12	87
MAGB 11.4 - Late granite																		
1.1	e,d,p,r	210.6	116.5	0.55	130	10	0.0019	0.51738	0.01441	16.01219	0.48670	0.22446	0.00206	2688	62	3013	15	89
2.1	e,d,eq,r	4638.8	1714.7	0.37	196	1414	0.1330	0.04128	0.00220	0.28914	0.03546	0.05080	0.00528	261	14	232	232	113
3.1	c,osc,p	53.7	55.8	1.04	27	16	0.0152	0.40230	0.01457	7.26567	0.34804	0.13099	0.00356	2180	67	2111	48	103
4.1	m,p	96.8	69.1	0.71	47	16	0.0083	0.42162	0.01411	7.96623	0.30462	0.13704	0.00202	2268	64	2190	26	104
5.1	e,d,p,r	2044.3	1271.1	0.62	129	284	0.0500	0.05468	0.00323	0.43568	0.03712	0.05779	0.00314	343	20	522	124	66
6.1	e,d,p,r	4108.7	3466.6	0.84	188	482	0.0570	0.04024	0.00234	0.30310	0.03405	0.05463	0.00487	254	15	397	213	64
7.1	c,osc,p	381.8	193.1	0.51	40	11	0.0058	0.10001	0.00271	0.81761	0.03315	0.05929	0.00160	614	16	578	60	106
7.2	c,osc,p	371.5	234.5	0.63	38	41	0.0239	0.09427	0.00141	0.79733	0.04339	0.06134	0.00310	581	8	651	112	89
8.1	c,hb,eq	116.9	94.3	0.81	48	12	0.0060	0.35369	0.01102	6.31838	0.23047	0.12956	0.00201	1952	53	2092	27	93
9.1	c,osc,p	258.1	113.5	0.44	26	13	0.0107	0.09951	0.00289	0.82700	0.04708	0.06028	0.00274	612	17	614	101	100
10.1	c,osc,p	77.1	37.1	0.48	33	17	0.0112	0.40078	0.00809	7.32359	0.19519	0.13253	0.00199	2173	37	2132	27	102
11.1	m,osc,d,p	542.7	69.8	0.13	54	16	0.0059	0.10446	0.00151	0.86146	0.02135	0.05981	0.00110	640	9	597	40	107
12.1	c,hb,p	62.5	48.2	0.77	20	14	0.0168	0.28125	0.00878	3.90206	0.27217	0.10062	0.00590	1598	44	1636	113	98
13.1	c,hb,p	48.8	16.6	0.34	17	11	0.0141	0.33541	0.00952	5.12446	0.28176	0.11081	0.00484	1865	46	1813	82	103

Labels: grain number.spot number
Site - p: prism (aspect ratio >2); eq: equant; e: end or edge; m: middle; r: overgrowth; c: core; fr: fragment
CL petrography - osc: oscillatory finescale zoning; sz: sector zoning; h: homogeneous; hb: homogeneous-bright; hd: homogeneous-dark; rex: recrystallised.
All analytical errors are 1 sigma.
207 Pb/206 Pb and 206 Pb/238 U ages are after correction for common Pb using measured 206 Pb/204 Pb and Cumming and Richards (1975) model Pb composition for the likely age of the rock.
f206 is the proportion of 206 Pb that is non-radiogenic (common) in origin, based on measured 204 Pb/206 Pb and Cumming and Richards (1975) Pb evolution.

images of representative grains in Fig. 5 and data are summarized in a concordia plot in Fig. 10). One core analysis has slightly discordant Archaean ages, with a $^{207}Pb/^{206}Pb$ one of *ca*. 3.0 Ga. Most of the remaining structural core analyses yielded close to concordant Paleoproterozoic ages, but with $^{207}Pb/^{206}Pb$, they dispersed beyond analytical error. These provide a weighted mean $^{206}Pb/^{207}Pb$ age of 2,137 ± 72 Ma (MSWD = 2.4). A group of outer

Table 2. Hf isotopic zircon data for Camboriú Complex rocks. Analytical errors are given at the two-sigma level

Grain/ spot	176 Hf/177 Hf	± 2 se	176 Lu/177 Hf	± 2 se	U-Pb Age (T1)	e Hf(0)	176 Hf/177 Hf	e Hf(t1)	$DM_{(T)}$	T DM (2)
ALBRUR 87 - Morro do Boi Migmatite (banded gneiss - mesosome)										
1.1	0.280993	0.000016	0.000896	0.000003	2957	-62.9	0.280942	1.9	0.281039	3179
2.1	0.280967	0.000020	0.000734	0.000013	2595	-63.8	0.280931	-6.9	0.281313	3463
3.1	0.281115	0.000022	0.000747	0.000003	2895	-58.6	0.281074	5.2	0.281086	2924
4.1	0.280898	0.000037	0.000676	0.000017	2921	-66.3	0.280860	-1.8	0.281066	3390
5.1	0.280949	0.000029	0.001009	0.000033	2842	-64.5	0.280894	-2.4	0.281126	3371
6.1	0.281107	0.000047	0.000984	0.000021	2955	-58.9	0.281051	5.8	0.281041	2931
7.1	0.280993	0.000029	0.000798	0.000012	2955	-62.9	0.280947	2.1	0.281041	3168
8.1	0.281333	0.000036	0.000694	0.000008	2860	-50.9	0.281295	12.3	0.281113	2440
4.1HF	0.281219	0.000038	0.000525	0.000009	2901	-54.9	0.281189	9.4	0.281082	2654
9.1	0.281055	0.000026	0.000471	0.000006	2901	-60.7	0.281029	3.7	0.281082	3021
10.1	0.280940	0.000020	0.000927	0.000015	2901	-64.8	0.280889	-1.3	0.281082	3340
11.1	0.281125	0.000057	0.000620	0.000002	2901	-58.2	0.281091	5.9	0.281082	2880
12.1	0.281065	0.000015	0.000712	0.000003	2901	-60.4	0.281025	3.6	0.281082	3031
MAGB 11.1 - Morro do Boi Migmatite (banded gneiss - mesosome)										
13.1	0.280975	0.000022	0.000372	0.000012	3037	-63.5	0.280954	4.2	0.280978	3093
1.1	0.281200	0.000021	0.000327	0.000002	1966	-55.6	0.281188	-12.2	0.281785	3316
2.1	0.281047	0.000024	0.001013	0.000070	1924	-61.0	0.281010	-19.4	0.281816	3738
3.1	0.281108	0.000022	0.000226	0.000001	3036	-58.8	0.281095	9.2	0.280979	2769
4.1	0.281029	0.000023	0.000752	0.000052	3330	-61.6	0.280981	12.1	0.280755	2810
12.1	0.281354	0.000019	0.000359	0.000001	2056	-50.2	0.281340	-4.7	0.281718	2915
5.1	0.280900	0.000017	0.000507	0.000006	3293	-66.2	0.280868	7.2	0.280783	3097
9.1	0.281070	0.000021	0.000388	0.000003	2993	-60.2	0.281047	6.5	0.281012	2911
8.1	0.280862	0.000050	0.000805	0.000011	3001	-67.5	0.280816	-1.5	0.281006	3433
6.1	0.280967	0.000018	0.000583	0.000019	3227	-63.8	0.280931	7.9	0.280833	3004
7.1	0.280837	0.000019	0.001351	0.000008	3327	-68.4	0.280751	3.8	0.280757	3341
15.1	0.280864	0.000020	0.001383	0.000051	3291	-67.5	0.280776	3.8	0.280785	3310
10.1	0.280980	0.000020	0.000311	0.000002	2922	-63.4	0.280962	1.8	0.281066	3158
11.1	0.281037	0.000018	0.000442	0.000007	2952	-61.4	0.281012	4.3	0.281043	3023
14.1	0.281043	0.000020	0.000638	0.000023	3050	-61.2	0.281005	6.4	0.280968	2966
MAGB 11.3 - Morro do Boi Migmatite (tonalitic vein - leucosome)										
1.1	0.280795	0.000021	0.000743	0.000006	2977	-69.9	0.280752	-4.4	0.281024	3595
4.1B	0.281435	0.000043	0.000897	0.000010	390	-47.3	0.281429	-39.0	0.282944	3750
10.1	0.280890	0.000030	0.000364	0.000010	2198	-66.5	0.280875	-18.0	0.281612	3858
2.2	0.281234	0.000017	0.000290	0.000002	643	-54.4	0.281230	-40.4	0.282760	4034
3.1	0.280816	0.000026	0.000461	0.000004	2963	-69.2	0.280790	-3.3	0.281035	3521
11.1	0.281242	0.000021	0.000540	0.000006	632	-54.1	0.281236	-40.4	0.282768	4029

Continue...

Table 2. Continuation

Grain/ spot	176 Hf/177 Hf	± 2 se	176 Lu/177 Hf	± 2 se	U-Pb Age (T1)	e Hf(0)	176 Hf/177 Hf	e Hf(t1)	$DM_{(T)}$	T DM (2)
7.1	0.280951	0.000029	0.000648	0.000009	2995	-64.4	0.280914	1.8	0.281010	3215
6.1	0.281950	0.000019	0.001050	0.000091	1195	-29.1	0.281927	-3.4	0.282356	2169
6.2B	0.282086	0.000051	0.000996	0.000012	919	-24.2	0.282069	-4.5	0.282559	2028
8.1B	0.281527	0.000022	0.000596	0.000009	247	-44.0	0.281524	-38.7	0.283047	3624
5.1	0.280878	0.000020	0.000308	0.000001	2969	-67.0	0.280860	-0.7	0.281030	3357
9.1	0.280818	0.000022	0.000396	0.000009	2850	-69.1	0.280796	-5.7	0.281120	3586
IC VII 75 - Ponta do Cabeço Leucogranite										
4.1	0.281283	0.000033	0.000455	0.000004	2081	-52.6	0.281265	-6.8	0.281699	3065
5.1	0.281431	0.000064	0.000519	0.000005	1940	-47.4	0.281412	-4.8	0.281805	2831
6.2B	0.281308	0.000044	0.000308	0.000003	2176	-51.8	0.281296	-3.5	0.281628	2932
6.1N	0.281003	0.000026	0.000642	0.000003	2914	-62.6	0.280967	1.8	0.281072	3154
9.1 B	0.281097	0.000040	0.000500	0.000002	2707	-59.2	0.281071	0.7	0.281229	3067
9.2 N	0.281090	0.000047	0.000582	0.000003	2699	-59.5	0.281060	0.1	0.281235	3097
9.3 B	0.281327	0.000036	0.000555	0.000003	2907	-51.1	0.281296	13.4	0.281077	2403
7.3	0.281039	0.000016	0.000450	0.000001	2950	-61.3	0.281013	4.3	0.281044	3022
7.1	0.281031	0.000021	0.000703	0.000004	2967	-61.6	0.280991	3.9	0.281031	3059
7.2	0.281268	0.000018	0.000634	0.000004	643	-53.2	0.281260	-39.3	0.282760	3971
3.1	0.281431	0.000023	0.000670	0.000003	879	-47.4	0.281420	-28.4	0.282588	3488
2.1	0.281429	0.000025	0.000438	0.000011	568	-47.5	0.281425	-35.2	0.282814	3658
1.1	0.281135	0.000028	0.000347	0.000001	2865	-57.9	0.281116	6.0	0.281109	2849
IC VII 79 - Ponta do Cabeço Granite (mafic xenolith)										
8.1	0.281954	0.000026	0.003207	0.000018	1541	-28.9	0.281861	2.0	0.282101	2088
4.1	0.281671	0.000020	0.001504	0.000018	587	-38.9	0.281655	-26.6	0.282801	3148
1.1	0.281976	0.000031	0.002997	0.000015	1534	-28.2	0.281889	2.9	0.282106	2029
2.1	0.281909	0.000019	0.002793	0.000021	1526	-30.5	0.281829	0.6	0.282112	2171
6.1	0.281911	0.000040	0.001937	0.000016	1512	-30.5	0.281855	1.2	0.282122	2120
12.1	0.281910	0.000045	0.003075	0.000024	1563	-30.5	0.281819	1.1	0.282085	2167
3.1	0.281869	0.000021	0.004258	0.000044	1579	-32.0	0.281741	-1.3	0.282073	2333
5.1	0.281878	0.000030	0.001311	0.000012	1563	-31.6	0.281839	1.8	0.282085	2122
9.1	0.281899	0.000030	0.001897	0.000027	1565	-30.9	0.281843	2.0	0.282083	2111
10.1	0.281958	0.000023	0.001827	0.000026	1497	-28.8	0.281906	2.7	0.282133	2015
11.1	0.281840	0.000029	0.003049	0.000050	1481	-32.9	0.281755	-3.1	0.282145	2367
7.1	0.281898	0.000021	0.003221	0.000096	1548	-30.9	0.281803	0.2	0.282096	2213
13.1	0.281894	0.000025	0.002721	0.000031	1563	-31.0	0.281814	0.9	0.282085	2180
MAGB 11.4 - Late granite										
2.1	0.281305	0.000014	0.003370	0.000030	261	-51.9	0.281289	-46.8	0.283037	4120
2.2	0.281139	0.000013	0.000465	0.000003	2200	-57.8	0.281119	-9.3	0.281610	3312

Continue...

Table 2. Continuation

Grain/ spot	176 Hf/177 Hf	± 2 se	176 Lu/177 Hf	± 2 se	U-Pb Age (T1)	e Hf(0)	176 Hf/177 Hf	e Hf(t1)	$DM_{(T)}$	T DM (2)
3.2	0.281015	0.000013	0.000614	0.000009	2111	-62.1	0.280991	-15.9	0.281677	3659
4.2	0.281050	0.000017	0.000592	0.000014	2190	-60.9	0.281025	-12.8	0.281618	3529
8.2	0.281390	0.000017	0.000425	0.000005	2092	-48.9	0.281373	-2.7	0.281691	2814
9.2	0.281546	0.000013	0.000824	0.000008	612	-43.4	0.281537	-30.2	0.282782	3391
10.2	0.281086	0.000018	0.000779	0.000005	2132	-59.6	0.281055	-13.1	0.281661	3503
11-2	0.281634	0.000017	0.001126	0.000018	640	-40.3	0.281620	-26.7	0.282762	3192
11.3	0.281571	0.000021	0.001861	0.000046	640	-42.5	0.281549	-29.2	0.282762	3348
12-2	0.281011	0.000015	0.000567	0.000002	1636	-62.3	0.280994	-26.6	0.282031	3958
13.2	0.281307	0.000014	0.000428	0.000006	1813	-51.8	0.281292	-12.0	0.281899	3185
14.2	0.281151	0.000031	0.000776	0.000015	2200	-57.3	0.281119	-9.3	0.281610	3313
15.2	0.281170	0.000025	0.000736	0.000009	2200	-56.6	0.281140	-8.5	0.281610	3267
16.2	0.280812	0.000015	0.001579	0.000041	3000	-69.3	0.280721	-4.9	0.281006	3649
17.2	0.281124	0.000014	0.000634	0.000008	2200	-58.3	0.281098	-10.0	0.281610	3361

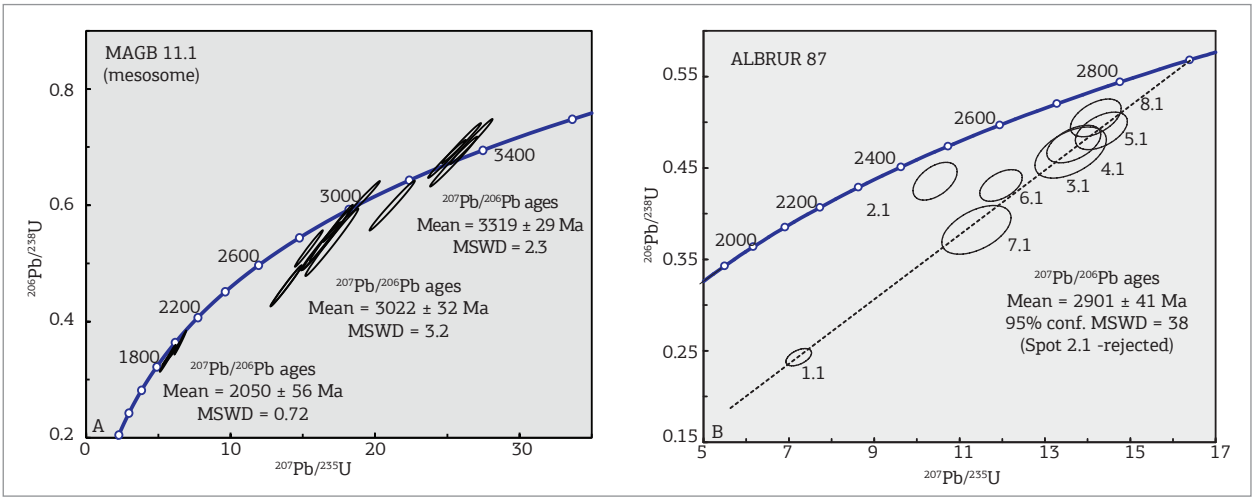

Figure 7. U-Pb concordia diagrams for paleosome of banded gneiss from Morro do Boi Migmatites. (A) Sample MAGB 11.1 and (B) ALBRUR 87. Analytical errors are depicted at the two-sigma level.

rims with concordant Neoproterozoic ages had a weighted mean $^{206}Pb/^{238}U$ age of 613 ± 23 Ma (MSWD = 0.03). Two analyses with ages between 2,100 to 1,600 Ma appear on the post-analysis inspection as composite core rim analyses, however they were not considered here. The 613 ± 23 Ma age is the intrusion age of the granite dike.

HF ISOTOPIC DATA

Hf data were obtained from the same zircons targeted in the SHRIMP U-Pb geochronology. The only exception to this is two grains from amphibolite sample IC VII 79. Given that this population is dominated by an igneous 1,563 Ma population, we are confident that an age of 1,563 Ma can be assigned in the assessment of these two Hf isotopic analyses. A total of 81 Hf isotopic determinations was carried out as follows: 28 on paleosome and 12 on leucosome of Morro do Boi migmatites; 26 in the amphibolite xenolith and in Ponta do Cabeço diatexite; and 15 in the later leucogranite dike. The Hf results are summarized in Tab. 2 and Fig. 11.

Hf isotopic data are very consistent, with Archean cores giving mostly positive but with some slightly negative

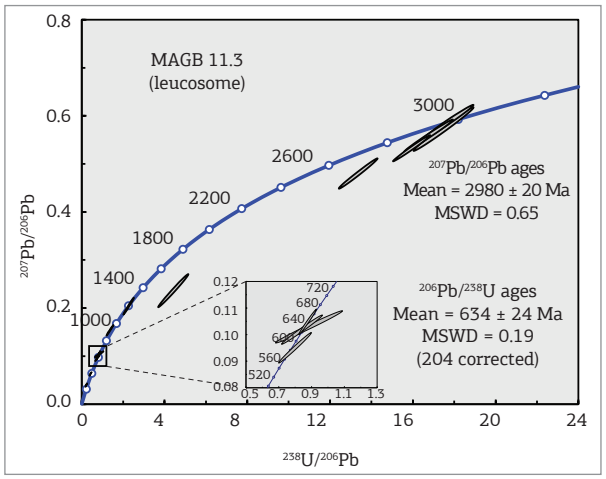

Figure 8. U-Pb concordia diagram for sample MAGB 11.3 of deformed leucosome in Morro do Boi migmatites. Analytical errors are depicted at the two-sigma level.

initial ε_{Hf} values (-2 to +10, with mean value *ca*. +4). Paleoproterozoic domains provide the same results as -0.5 to -16 with a mean value of *ca*. -8. The Neoproterozoic domains yielded highly negative ε_{Hf} values of -25 to -40.

The $Hf_{(TDM2)}$ model ages for zircons from the Archean rocks and Mesoproterozoic amphibolitic xenolith were close to the values of U-Pb ages, therefore these rocks possibly represent the addition of juvenile material to the crust, whereas the Paleoproterozoic and Neoproterozoic overgrowths indicate much older Hf model ages, characterizing the predominance of crustal reworking processes in these eras. On the other hand, the igneous zircons from the *ca*. 1,563 Ma amphibolite enclave (probably a dismembered mafic dike) yielded slightly positive initial ε_{Hf} values of up to +4.

DISCUSSION

U-Pb zircon ages

The U-Pb zircon ages can be directly correlated to the different overgrowth phases observed in the zircons and can reflect the very long crustal history for the Camboriú Complex. This process, recorded in zircon cores, started at 3.3 Ga, continued during the rest of the Archean, with events between 3.0 and 2.7 Ga, and was followed by an important migmatization phase in the Paleoproterozoic (from 2.1 to 1.9 Ga). During the Mesoproterozoic at ca 1.56 Ga, a crustal extension occurred, which was characterized by basic dike intrusions now preserved as disrupted mafic bands in the migmatites and xenoliths in Ponta do Cabeço diatexite. In the Neoproterozoic, between 0.64 and 0.59 Ga, the migmatites underwent a new thermal event at high-amphibolite facies conditions that enabled melting to different degrees of preexisting rocks, generating the banded migmatites in their present form and Ponta do Cabeço Granite diatexite. The U-Pb age probability density plot (Fig. 12) demonstrates these episodic events.

Hf isotopic data

The old U-Pb ages correspond to dominantly positive ε_{Hf} values (-2 to +10) and model ages that are close to zircon U-Pb values. This shows the important juvenile crustal accretion in the Archean. In the Paleoproterozoic, tectonothermal processes involved its crust reworking without juvenile additions. This is demonstrated by the negative initial ε_{Hf} values (-0.5 to -16). Crustal reworking also took place during the Neoproterozoic, as indicated by even more negative ε_{Hf} values, between -25 and -40 for 650 to 600 Ma zircon components.

An exception to this scenario is characterized by the values obtained for the amphibolite xenolith, with 1,563 Ma magmatic zircon with positive initial ε_{Hf} values around +2. This indicates minor juvenile crustal addition occurred at *ca*. 1,563 Ma. On the other hand, the only amphibolite zircon domain dated 0.59 Ga yielded a very negative initial ε_{Hf} value around -26, which is compatible with what was observed in the crystals of the same age from the host diatexitic granitoid matrix.

Polycyclic crustal evolution

The polycyclic evolution of the complex is summarized in the zircon age histogram of Fig. 12, whereas the ε_{Hf} – time plot (Fig. 11) shows that most crust was formed in the Archean and then was repeatedly reworked up to the Neoproterozoic.

The intensity of the Neoproterozoic deformation and remobilization with melt domains masked the original characteristics of the old protoliths. The degree of mobilization was to such an extent that melts migrated outwards and penetrated the Neoproterozoic Brusque Group metasedimentary rocks. The final Neoproterozoic evolution of the complex is linked with the regional thermal peak responsible for the emplacement of the granitoids in Brusque Group, in particular the Valsungana Granite. Because of this last major remobilization, we prefer to regard the Complex in its present form as a Neoproterozoic unit, albeit it contains large volumes of older crustal material.

Regional correlation and tectonic significance

It is very difficult to correlate the Camboriú Complex with its adjacent gneissic-migmatitic terranes in southeastern

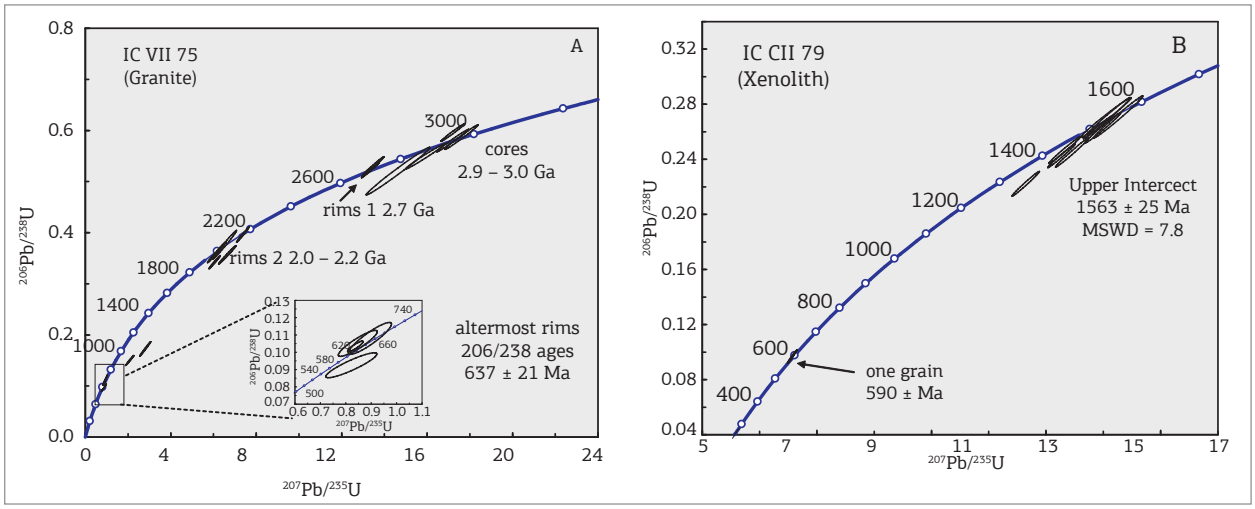

Figure 9. U-Pb concordia diagrams for (A) sample IC VII 75 of Ponta do Cabeço diatexitic granitoid neosome and (B) IC VII 79 of amphibolite xenolith. Analytical errors are depicted at the two-sigma level.

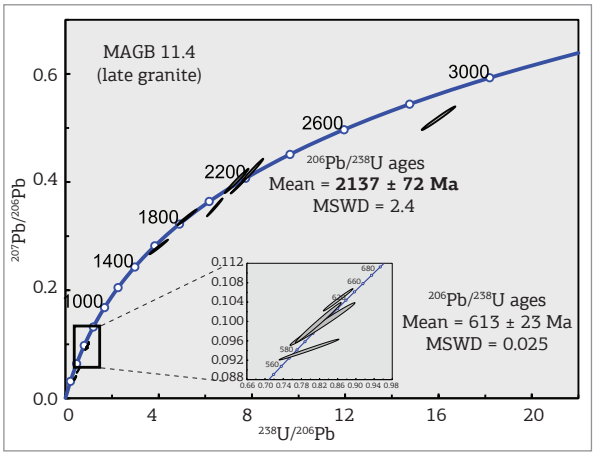

Figure 10. U-Pb concordia diagram for sample MAGB 11.4 of discordant granite sheet cutting migmatites. Analytical errors are depicted at the two-sigma level.

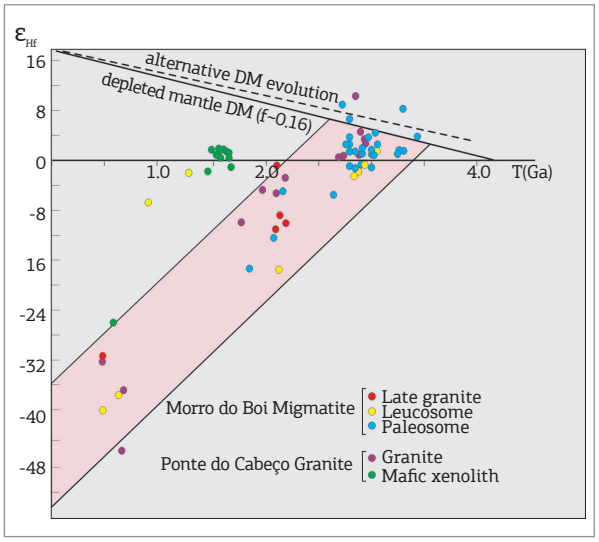

Figure 11. Initial ε_{Hf} values – time plot. Note that the evolution trend of the Archean zircons coincides with the initial ε_{Hf} values of Paleoproterozoic and Neoproterozoic ages. On the other hand, the igneous zircons from a *ca.* 1560 Ma basic rock show more juvenile and positive initial ε_{Hf} values.

South America, such as the Luis Alves Microplate (Basei *et al.* 2009) and Río de La Plata Craton (Rapela *et al.* 2007, Oyhantçabal *et al.* 2011). For these domains, especially the Luis Alves Microplate, basement gneisses that represent the closest and largest exposures of similar rocks outside the Camboriú Complex, ages of > 2.9 Ga (such as those in the Camboriú Complex), are unknown. Additionally, granulite-facies gneisses, which are lacking in Camboriú Complex, predominate in these other basement occurrences.

The most likely correlative unit is the Atuba Complex migmatites (Siga Jr. *et al.* 1995, Sato *et al.* 2003), which occurs between the Luis Alves Microplate and the Ribeira Belt. Besides the geologic similarities, zircon U-Pb ages in the 3.3 to 2.9 Ga and 2.1 to 2.0 Ga intervals are observed for inherited components in leucosomes and Neoproterozoic granitoids in the Atuba Complex (Sato & Siga Jr. 2001, Sato *et al.* 2003). In the Nico Perez Terrane domains, Hartmann *et al.* (2001) obtained zircon ages older than 3.0 Ga, making this segment another possible correlation. However, little is known about the Nico Perez domains, which makes further comparison difficult.

The origin of old rocks that compose part of the Camboriú Complex favored in this paper formed a strongly reworked exotic small continental fragment, which was involved in the Neoproterozoic amalgamation processes that led to the formation of the Dom Feliciano Belt during the construction of Western Gondwana.

Fabric analysis integrated with moderate to high pressures (> 8 Kbar) in the migmatites suggests that

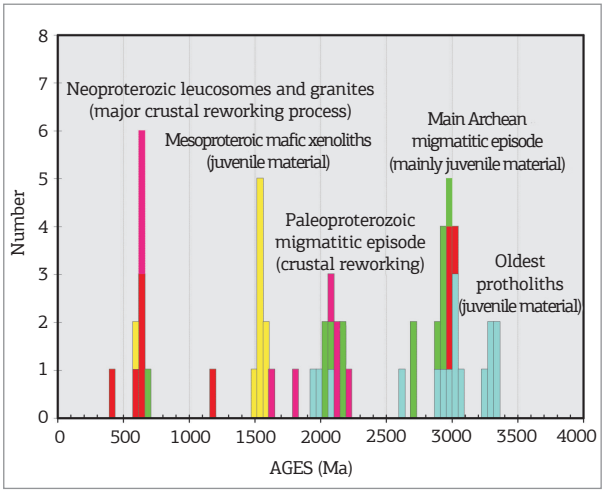

Figure 12. Probability density plot for U-Pb zircon ages from Camboriú Complex.

migmatization happened in thickened crust, with flowed laterally along the orogen trend. Therefore, it might indicate lateral escape of high temperature deep thickened crust subsequent to initial collision, analogous to what is now happening beneath the Tibetan Plateau.

CONCLUSIONS

The Camboriú Complex shows a protracted history of magmatic and high-temperature tectonothermal events, starting at *ca*. 3.3 Ga, and continuing at 3.0 – 2.9, 2.7, 2.1 – 1.9, 1.56, and 0.64 – 0.61 Ga. Repeated high-temperature mobilization resulted in the lithological complexity of migmatites, including in the Neoproterozoic, when mobilization was to the extent that melts escaped from the Complex and penetrated adjacent Neoproterozoic supracrustal rocks.

Zircon Hf isotopic analysis integrated with the U-Pb geochronology shows that juvenile crustal accretion is largely restricted to the Archean, with the Paleo- Neoproterozoic migmatization events being marked by intra-crustal mobilization of the Archean components. The only exception to this is a suite of basic bodies interpreted as originally dikes, which were emplaced into the Complex at *ca*. 1.56 Ga.

The Camboriú Complex is probably an exotic continental fragment rafted in from the East and attached to Western Gondwana during the closure of a Neoproterozoic ocean basin. Based on similar U-Pb zircon ages, it might be correlated with the Atuba Complex, another continental fragment in the Neoproterozoic orogenic belts in Southern Brazil.

Neoproterozoic mobilization seems to have involved lateral movement along the trend of the orogenic belt. This might mean lateral escape of hot, partially melted crust following initial collision of continental terranes.

ACKNOWLEDGEMENTS

The authors are grateful to colleagues from the University of São Paulo (USP) for the fruitful discussions and help during the analysis. Most of laboratory analysis and fieldwork were supported by grants from the São Paulo State Foundation of Research Support (FAPESP – 2005/58688-1).

REFERENCES

Almeida F.F.M., Hasui Y., Brito Neves B.B., Fuck R.A. 1981. Brazilian Structural Provinces; an introduction. *Earth Science Reviews*, **17**:1-29.

Basei M.A.S. 1985. *O Cinturão Dom Feliciano em Santa Catarina*. Unpublished PhD. thesis, University of São Paulo, São Paulo, 191p.

Basei M.A.S., Brito Neves B.B., Siga Jr. O., Babinski M., Pimentel M.M., Tassinari C.C.G., Hollanda M.H.B., Nutman A.P., Cordani U.G. 2010. Contribution of SHRIMP U-Pb zircon geochronology to unravelling the evolution of Brazilian Neoproterozoic fold belts. *Precambrian Research*, **183**:112-144. doi: I 10.1016/j.precamres.2010.07.015

Basei M.A.S., Frimmel H.E., Nutman A.P., Preciozzi F. 2008. West Gondwana amalgamation based on detrital zircon ages from Neoproterozoic Ribeira and Dom Feliciano belts of South America and comparison with coeval sequences from SW Africa. In: Pankhurst R.J., Trouw R.A.J., Brito Neves B. B., Wit M.J. (eds) *West Gondwana*: Pre-Cenozoic Correlations Across the South Atlantic Region. Geological Society London Special Publication, **294**:239-256.

Basei M.A.S., Frimmel H.E., Nutman A.P., Preciozzi F., Jacob J. 2005. The connection between the Neoproterozoic Dom Feliciano (Brazil/Uruguay) and Gariep (Namibia/South Africa) orogenic belts. *Precambrian Research*, **139**:139-221.

Basei M.A.S., Nutman A., Siga Junion O., Passarelli C., Drukas C.O. 2009. The evolution and tectonic setting of the Luís Alves microplate of southeastern Brazil: an exotic terrane during the assembly of western Gondwana In: Gaucher C., Sial A.N., Halverson G.P., Frimmel H.E. (eds) *Neoproterozoic Tectonics, Global Change and Evolution*: A Focus on Southwestern Gondwana. Amsterdam: Elsevier, pp. 273-291.

Basei M.A.S., Siga Jr. O., Masquelin H., Harara O.M., Reis Neto J.M., Preciozzi F. 2000. The Dom Feliciano Belt of Brazil and Uruguay and its Foreland Domain the Rio de la Plata Craton: framework, tectonic evolution and correlation with similar provinces of Southwestern Africa. In: Cordani U.G., Milani E.J., Thomaz Filho A., Campos D.A. (eds) *Tectonic Evolution of South America*, p. 311-334.

Bittencourt M.F. & Nardi L.S.V. 2004. The role of xenoliths and flow segregation in the genesis and evolution of the Paleoproterozoic Itapema Granite, a crustally derived magma of shoshonitic affinity from southern Brazil. *Lithos*, **73**:1-19.

Blichert-Toft J. & Albarede F. 1997. The Lu-Hf isotope geochemistry of chondrites and the evolution of themantle-crust system. *Earth and Planetary Sciences Letters*, **148**:243-258.

Compston W., Williams I.S., Meyer C. 1984. U-Pb geochronology of zircons from lunar breccia 73217 using a sensitive high mass-resolution ion microprobe. *Journal of Geophysical Research*, **89**:525-534.

Cumming G.L. & Richards J.R. 1975. Ore lead isotope ratios in a continuously changing Earth. *Earth and Planetary Science Letters*, **28**:155-171.

Griffin W.L., Belousova E.A., Shee S.R., Pearson N.J., O'Reilly S.Y. 2004. Archean crustal evolution in the northern Yilgarn Craton: U-Pb and Hf isotope evidence from detrital zircons. *Precambrian Research*, **131**:231-282.

Hartmann L.A., Bitencourt M.F., Santos J.O.S., McNaughton N.J., Rivera C.B., Betiollo L. 2003. Prolonged Paleoproterozoic magmatic participation in the Neoproterozoic Dom Feliciano Belt, Santa Catarina, Brazil, based on zircon U-Pb SHRIMP geochronology. *Journal of South American Earth Sciences*, **16**:477-492.

Hartmann L.A., Campal N., Santos J.O., MacNaughton N.J., Schipilov A. 2001. Archean crust in the Rio de la Plata Craton, Uruguay: SHRIMP U-Pb reconnaissance geochronology. *Journal of South American Earth Sciences*, **14**:557-570.

Lopes A.P. 2008. *Geologia do Complexo Camboriu, SC*. Unpublished PhD. thesis, University of São Paulo, São Paulo, Brazil.

Ludwig K.R. 2001. *Using Isoplot/Ex*. A geochronological toolkit for Microsoft Excel. Berkeley Geochronology Center, Special Publications No. 1, Berkeley, USA.

McClaren A.C., FitzGerald J.D., Williams I.S. 1994. The microstructure of zircon and its influence on the age determination from Pb/U isotopic ratios measured by ion microprobe. *Geochimica Cosmochimica Acta*, **58**:993-1005.

Oyhantçabal P., Siegesmund S., Wemmer K. 2011. The Rio de La Plata Craton: a review of units, boundaries, ages and isotopic signature. *International Journal of Earth Sciences*, **100**:201-220.

Patiño Douce A.E. 2005. Vapor-absent melting of tonalite at 15-32 kbar. *Journal of Petrology*, **46**:275-290.

Phillip R.P., Mallmann G., Bitencourt M.F., Souza R.R., Liz J.D., Wild F., Arend S., Oliveira A.S., Duarte L.C., Rivera C.B., Prado M. 2004. Caracterização Litológica e Evolução Metamórfica da Porção Leste do Complexo Metamórfico Brusque, Santa Catarina. *Revista Brasileira de Geociências*, **34**:21-34.

Phillip R.P., Massonne H.J., Theye T., Campos R.S. 2009. U-Th-Pb EMPA Geochronology of polygenetic monazites of the metapelitic migmatitic gneisses of Camboriu Complex, SC, Southern Brazil: evidences for the collisional and post-collisional events in the Dom Feliciano Belt. Simpósio 45 anos de Geocronologia no Brasil, *Boletim de Resumos Expandidos*, São Paulo, Brasil, p. 289-291.

Poli S. & Schmidt M.W. 2004. Experimental subsolidus studies on epidote minerals. *Reviews of Mineralogy and Geochemistry*, **56**:171-195.

Rapela C.W., Pankhurst R.J., Casquet C., Fanning C.M., Baldo E.G., Gonzalez-Casado J.M., Galindo C. Dahlquist J. 2007. The Rio de La Plata craton and the assembly of SW Gondwana. *Earth Sciences Review*, **83**:49-82.

Sato K., Basei M.A.S., Ferreira C.M., Vlach S.R.F., Ivanuch W., Siga Jr. O., Onoi A.T. 2010. *In situ U-Th-Pb isotopic analyses by Excimer laser ablation/ICP–MS on Brazilian xenotime megacrystal: first U-Pb results at CPGeo-IG-USP*. VII SSAGI, Brasília, DF, CD Room.

Sato K., Siga Jr. O. 2001. Rapid grouth of continental crust between 2.2-1.8 Ga in the South American platform. *Gondwana Research*, **5**:165-173.

Sato K., Siga Jr. O., Nutman A.P., Basei M.A.S., McReath I., Kaulfuss G.A. 2003. The Atuba Complex, Southern South American Plataform: Archean components and Paleoproterozoic to Neoproterozoic tectonothermal events. *Gondwana Research*, **6**:251-263.

Sato K., Siga Jr. O., Silva J.A., McReath I., Liu D., Iizuka T., Rino S., Hirata T., Sproesser W.M., Basei M.A.S. 2009. In Situ Isotopic Analyses of U and Pb in Zircon by Remotely Operated SHRIMP II, and Hf by LA-ICP-MS: an Example of Dating and Genetic Evolution of Zircon by 176Hf/177Hf from the Ita Quarry in the Atuba Complex, SE Brazil. *Geol. USP, Série Cientifica São Paulo*, **9**:61-69.

Sawyer E.W. 2008a. Working with migmatites: Nomenclature for the constituent parts. Sawyer E.W., Brown M. (eds) *Working with Migmatites*. Mineralogical Association of Canada, Short Courses Series, **38**:1-28.

Sawyer E.W. 2008b. *Atlas of Migmatites*. The Canadian Mineralogist, Special Publication, **9**:371.

Siga Junior O., Basei M.A.S., Reis Neto J.M., Machiavelli A., Harara O.M.M. 1995. O Complexo Atuba: um Cinturão Paleoproterozóico intensamente retrabalhado no Neoproterozóico. *Geologia USP: Série Científica*, **26**:69-98.

Silva L.C., Hartmann L.A., McNaughton N.J., Fletcher I. 2000. Zircon U-Pb SHRIMP dating of a Neoproterozoic overprint in Paleoproterozoic granitic-gneissic terranes, Southern Brazil. *American Mineralogist*, **85**:649-667.

Silva L.C., McNaughton N.J., Armstrong R., Hartmann L.A., Fletcher I.R. 2005a. The Neoproterozoic Mantiqueira Province and its African connections: a zircon-based U–Pb geochronologic subdivision for the Brasiliano/Pan-African system of orogens. *Precambrian Research*, **13**:203-240.

Silva L.C, McNaughton N.J., Fletcher I. 2005b. Reassesment on complex zircon populations from Neoproterozoic granites in Brazil, through SEM imaging and SHRIMP analyses: consequences for discrimination of emplacement and inherited ages. *Lithos*, **82**:503-525.

Silva L.C., McNaughton N.J., Hartmann L.A., Fletcher I.R. 2003. Contrasting zircon growth patterns in Neoproterozoic granites of Southern Brazil revealed by SHRIMP U-Pb analyses and SEM imaging: consequences for the discrimination of emplacement and inheritance ages. In: IV South American Symposium on Isotope Geology, Salvador, Bahia, Brazil. *Short papers*, p. 687-690.

Sircombe K.N. 2000. Quantitative comparison of large data sets of geochronological data using multivariate analysis: a provenance study example from Australia. *Geochimica et Cosmochimica Acta*, **64**:1593-1616.

Söderlund U., Patchett J.P., Vervoort J.D., Isachsen C.E. 2004. The ^{176}Lu decay constant determined by Lu-Hf and U-Pb isotope systematics of Precambrian mafic intrusions. *Earth and Planetary Science Letters*, **219**:311-324.

Stern R.A. 1998. High resolution SIMS determination of radiogenic trace-isotope ratios in minerals. In: Cabri L.J. & Vaughan D.J. (eds) *Modern Approches to Ore and Environmental mineralogy*. Short Course Series, Mineralogical Association of Canada, p. 241-268.

Vlach S.R.F., Basei M.A.S., Castro N.A. 2009. Idade U-Th-Pb de monazita por microssonda eletrônica do Granito Nova Trento, Grupo Brusque, SC. Simpósio 45 anos de Geocronologia no Brasil. *Boletim de Resumos Expandidos*, São Paulo, Brasil, p. 325-327.

Williams I.S. 1998. U-Th-Pb geochronology by ion microprobe. In: McKibben M.A., Shanks III W.C., Ridley W.I. (eds) Applications of microanalytical techniques to understanding mineralising processes. Society of Economic Geologists. *Reviews in Economic Geology*, **7**:1-35.

Arquivo digital disponível on-line no site www.sbgeo.org.br